Depletion-Induced Tunable Assembly of Complementary Platonic Solids

Rahul Nag, Nina Rouvière, Jaime Gabriel Trazo, Jules Marcone, Nika Kutalia, Claire Goldmann, Marianne Impéror-Clerc, Damien Alloyeau, Doru Constantin, Cyrille Hamon

Depletion-Induced Tunable Assembly of Complementary Platonic Solids

Rahul Nag,[1] Nina Rouvière,[2] Jaime Gabriel Trazo,[1] Jules Marcone,[1] Nika Kutalia,[1] Claire Goldmann,[1] Marianne Impéror-Clerc,[1*] Damien Alloyeau,[3*] Doru Constantin,[2*] Cyrille Hamon[1*]

[1] Laboratoire de Physique des Solides, Université Paris-Saclay, CNRS, Orsay 91405, France.

[2] Institut Charles Sadron, CNRS and Université de Strasbourg, 67034 Strasbourg, France

[3] Laboratoire Matériaux et Phénomènes Quantiques, Université Paris Cité - CNRS, Paris,

Abstract.

Multicomponent self-assembly has been explored to create novel metamaterials from nanoparticles of different sizes and compositions, but the assembly of nanoparticles with complementary shapes remains rare. Recent binary assemblies were mediated by DNA base pairing or induced by solvent evaporation. Here, we introduce depletion-induced self-assembly (DISA) as a novel approach for constructing tunable binary lattices. *In situ* structural analysis in the real and the reciprocal spaces demonstrates DISA of a binary mixture of octahedra and tetrahedra into extended supercrystals with $Fm\bar{3}m$ symmetry. The inter-particle distance, adjustable by depletant concentration, offers a versatile method for assembling nanoparticles into ordered structures while they remain dispersed in a liquid phase. We show that DISA can control the packing fraction of such binary supercrystals between φ=0.37 and φ=0.66, much lower than dense packing in the dry state. These findings highlight DISA's potential for creating complex and highly ordered metamaterials with tailored properties.

Keywords: binary assembly, octahedra, tetrahedra, Liquid cell TEM, Small Angle X-Ray Scattering, gold nanoparticles

Corresponding authors:

Marianne Impéror-Clerc : marianne.imperor@cnrs.fr

Damien Alloyeau : damien.alloyeau@univ-paris-diderot.fr

Doru Constantin : constantin@unistra.fr

Cyrille Hamon : cyrille.hamon@cnrs.fr

Filling a box with geometric shapes is a longstanding problem that has puzzled scientists of all ages. In mathematics, the "box" is the three-dimensional flat space (Euclidean $\mathbb{R}^3$), which can be filled with one or more shapes. The key rule is that the pattern propagates in all directions without any gaps or overlaps. Among Platonic solids, the cube is a space-filling polyhedron, whereas the tetrahedra and octahedra are not. Indeed, the dihedral angles of tetrahedra and octahedra are not commensurable with 2π, and as a consequence they do not fill the Euclidian space without gaps. However, their sum is. In this sense, these two Platonic solids are complementary in shape. As a result, a mixture of regular tetrahedra and octahedra with identical edge length and with a 2:1 number ratio can fill the Euclidian $\mathbb{R}^3$ by forming a face-centered cubic (FCC) lattice.[1, 2] This arrangement corresponds to the structure formed by the two coordination polyhedrons in the well-known FCC packing of spheres, resulting in octahedral and tetrahedral cavities. In this binary space-filling structure, all octahedrons have the same orientation and are edge-sharing, leaving space in between for tetrahedra, which exhibit two different but equally probable orientations. Each octahedron shares its eight faces with eight tetrahedra, while each tetrahedron shares its four faces with four octahedra. This configuration results in a volume fraction of one, as expected for a space-filling arrangement. This pattern can be found at all scales, from the arrangement of atoms to the construction of Fuller's octet-truss frame structure,[3] being used in different applications such as additive manufacturing or else in the architecture of larger structures. However, engineering such patterns with nanoparticles (NPs) at the mesoscale remains a challenge.

Multicomponent self-assembly enables the combination of nanoparticles (NPs) with varying sizes and compositions to yield metamaterials that possess properties distinct from those of their single-component counterparts.[4-7] In addition to favorable pairwise interactions, a binary assembly forms if its packing fraction exceeds those of the unary structures.[5] Spherical NPs have been extensively studied for the formation of multicomponent self-assembly.[8-11] While there have been some successful realizations of co-assembly involving anisotropic shapes with isotropic ones,[12-16] the creation of anisotropic shape alloys co-assembling two different anisotropic nanoparticles remains less common. For instance, the group of C. Murray have reported binary assemblies of gadolinium nanoplates with complementary shapes.[17] The groups of M. Bodnarchuk and M. Kovalenko have reported the binary and ternary assembly of perovskite NPs with various shapes.[18-20] In these works the assembly was performed by the slow evaporation of the solvent. In 2024, the groups of S. Glotzer and C. Mirkin have reported a variety of shape-complementary polyhedra space-filling assemblies, including binary

mixtures of tetrahedra and octahedra, mediated with DNA base pairing.[21] In this latter approach, the binary assembly can only be obtained when the two shapes are functionalized with complementary DNA strands. Moreover, once assembled, the lattices were not reconfigurable due to the strong interaction induced by solvent evaporation or DNA base pairing. In this work, we introduce depletion-induced self-assembly (DISA) as a strategy of building binary lattices with tunable lattice parameters.

Hard polyhedra tend to align along their facets to maximize entropy and minimize free energy, a phenomenon described as directional entropic forces.[22-24] In depletion-induced self-assembly, the interaction is also of entropic nature but comes from the depletants (micelles, polymers), since maximization of their free available volume increases the overall entropy of the system.[25] DISA is routinely used to separate plasmonic nanoparticles (NPs) of different shapes,[26, 27] but is less frequently employed for creating supercrystals in suspension.[28-30] One advantage of DISA is the possibility to conveniently tune the inter-NPs distance by controlling the depletant concentration, as shown for triangular nanoplates stacks.[31] However, since the assemblies are dispersed in a liquid phase, standard electronic microscopy techniques cannot be used to describe the structure of the materials directly in solution. DISA has been used to assemble microparticles with complementary shapes but not yet NPs,[32, 33] a strategy that might seem counterintuitive to the NPs community because DISA is generally used for shape separation.

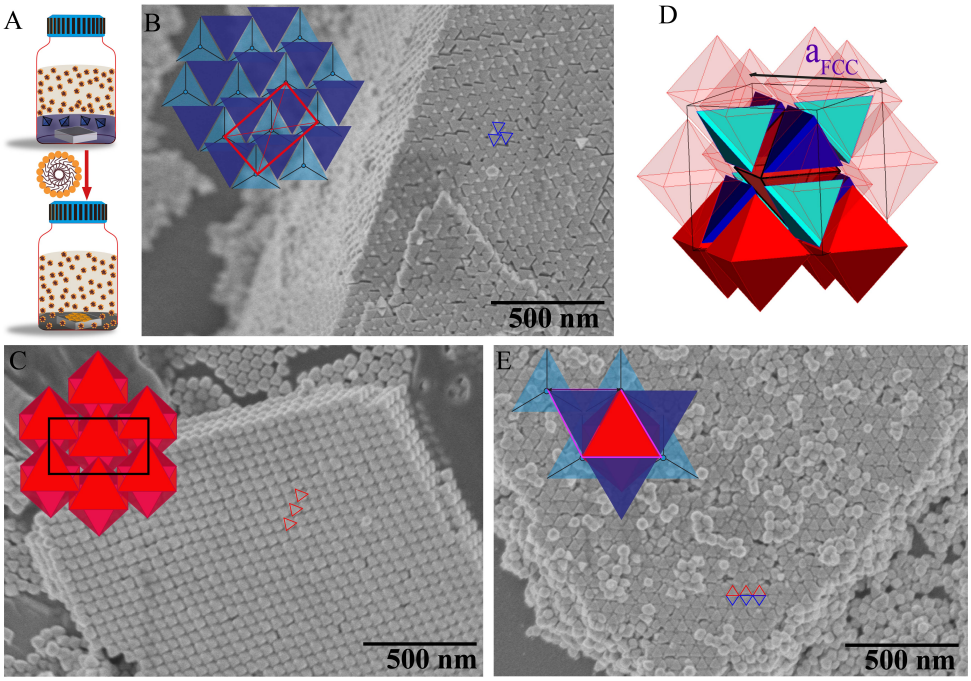

Figure 1: Binary Assembly by DISA. (A) An illustration of the DISA process using CTAC as depletant and a Si wafer at the bottom of the vial for the deposition of the supercrystals. SEM

micrographs of the supercrystals produced by DISA: (B)Au-Td, (C) Au-Oct and (E) the binary assembly at 2:1 stoichiometry. (Scale bar = 500 nm) The insets show the schematic of the respective 2D-unit cell in a single monolayer of NPs. (D) Schematic diagram of the 3D FCC unit cell of the binary mixture containing 4 octahedra and 8 tetrahedra. All octahedra (in red) are equivalent by translation. Tetrahedra have 2 different and equi-probable orientations, shown respectively in dark blue and light blue.

Here we show the formation of binary lattices of tetrahedra and octahedra mediated by DISA (**Figure 1**). We combined *ex situ* characterization of the lattices with two complementary *in situ* techniques: synchrotron based Small Angle X-ray scattering (SAXS) and liquid-cell transmission electron microscopy (LCTEM). Gold NPs were prepared by seed-mediated growth in water, using cetyltrimethylammonium chloride (CTAC) as stabilizer. Specifically, polyhedra of similar edge length (E.L) were prepared: octahedra (Oct, Au-Oct_{52}) of E.L= 52.4 ± 2.62 nm and tetrahedra (Td, Au-Td_{50}) of E.L 50.3 ± 1.91 nm which takes into account a small truncation. Full characterization of the NPs is provided in the Supporting Information (**Figure S01-S02, Table S1**). We measured the Au^0 concentration from the absorbance at 400 nm to determine the concentration of NPs.[34] This allowed us to prepare mixtures with a 2:1 ratio of tetrahedra to octahedra, which is the sweet-spot for the formation of the binary assembly, over other stoichiometry (**Figure S03**).

We first collected supercrystals formed by DISA on a Si wafer (**Figure 1A**) to characterize them *ex situ* by scanning electron microscopy (SEM). Unary tetrahedra and octahedra supercrystals were identified by optical microscopy (**Figure S04**). These supercrystals adopted triangular or rhomboidal shapes with typical sizes of a few microns and exhibited corresponding triangle and rhombus facets on the substrate. SEM images revealed that the tetrahedra crystallized into a periodic stack of dense monolayers, with each monolayer displaying a centered rectangular lattice symmetry (**Figure 1B, Figure S05**).[35] In contrast, the octahedra packed into dense monolayers consistent with previously reported supercrystals exhibiting C2/m monoclinic lattice symmetry (**Figure 1C, Figure S06**).[36] The packing fraction for the observed unary supercrystals is about φ=0.61 for tetrahedra and φ=0.89 for octahedra. Packing fraction are always compared for nanoparticles without truncation. In contrast, the FCC binary lattice of tetrahedra and octahedra optimizes both the packing fraction (φ=1) and the overlap between the triangular facets of these particles, explaining its stability.

The binary lattice typically displayed triangular patterns on the SEM images (**Figure 1D-E, Figure S07**), different from the arrangements found in the unary lattices. Although the

formation of the binary lattice is identified by SEM (**Figure 1D-E, Figure S07-S08**), we further validated this result *in situ* using SAXS and LCTEM (**Figure 2**).

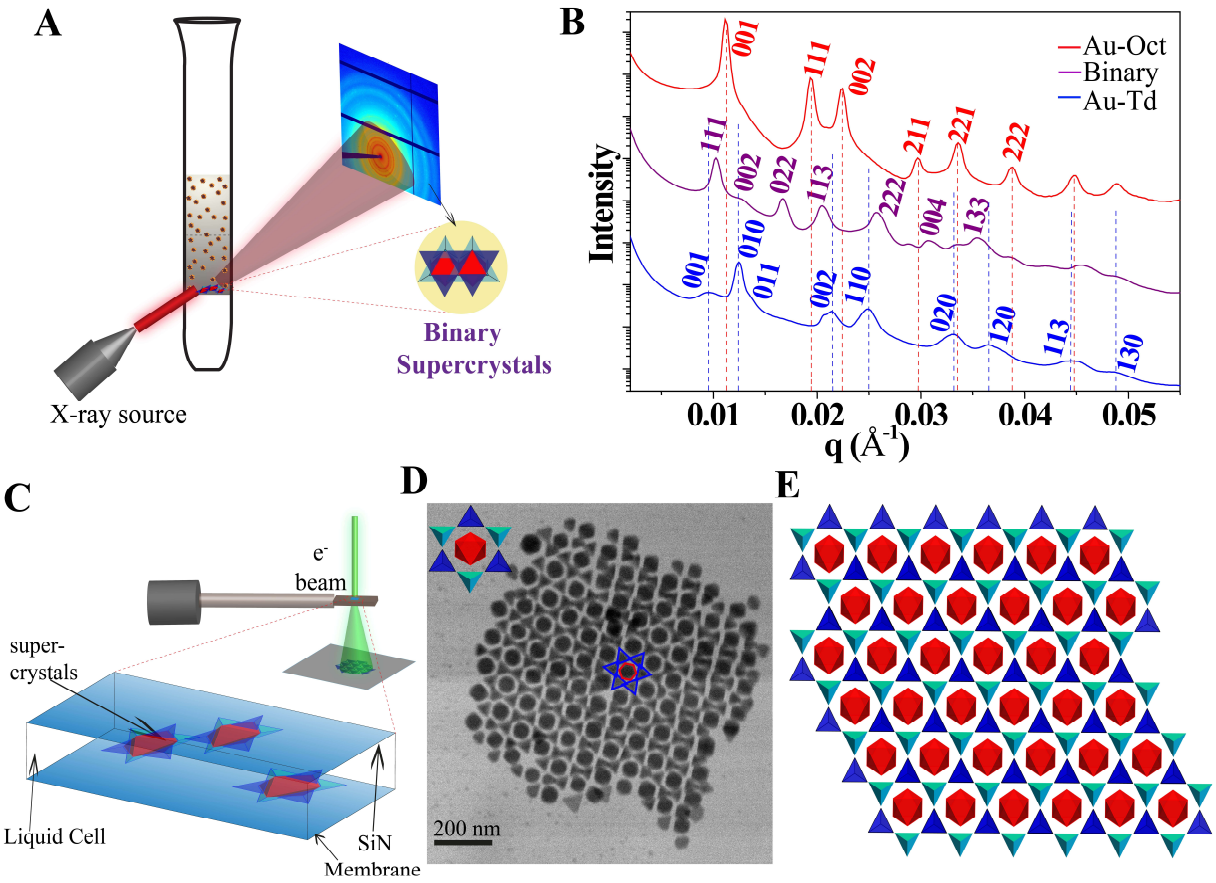

Figure 2: Characterization of the binary assembly *in situ*. (A) Schematic diagram of the depletion-induced self-assembly of the NPs and their detection by SAXS inside a glass capillary. (B) 1D-SAXS pattern of the Au-Oct$_{52}$ (red), Binary (violet) and Au-Td$_{50}$ (blue) with the indexing of the Bragg peaks. CTAC concentration was 450 mM and coresponding a_{FCC} of the binary lattice (violet curve) is 105.8 nm. (C) Illustration of the *in-situ* TEM observation of the supercrystals in LCTEM. (D) LCTEM micrograph of the binary assembly (Scale bar =200 nm). CTAC concentration was 150 mM. (E) Schematic representation of a monolayer of the binary assembly viewed along a <111> direction as observed in LCTEM.

For SAXS, the colloidal supercrystals are formed in glass capillaries by DISA and analyzed *in situ* (**Figure 2A-B, S09-S10**). Sharp Bragg peaks indicate the formation of extended lattices and their indexing confirms the lattice symmetry of the supercrystals. The diffractogram of the binary lattice displays peaks at different positions compared to both lattices made solely of tetrahedra or octahedra, revealing the formation of a new structure, with no trace of the peaks of unary supercrystals. The peak progression agrees with an FCC structure exhibiting $Fm\bar{3}m$

symmetry, in line with the binary supercrystal depicted in **Figure 1D**. We then studied the unary and binary supercrystals by low-dose LCTEM confined between two SiN membranes with 500 nm spacers. We mainly observed assemblies consisting of one monolayer laying on the SiN membrane (**Figure 2C-E, S11 and S12**), but some supercrystals with few layers stacking perpendicularly to the membrane were also observed (**Figure S13**). The reduced ability of confined supercrystals to stack perpendicularly to the membrane is due to the affinity of NPs for the liquid-cell windows, but, as we previously evidenced with other entropy-driven supercrystals, their lower dimensionality does not affect their crystal lattice.[37] Indeed, the binary monolayers show one octahedron surrounded by six tetrahedra (**Figure 2E**), as expected for the FCC lattice oriented in the ⟨111⟩ direction and the 3D stacking (**Figure S13**) agrees with the model structure in **Figure 1D**. This synergy between reciprocal and real space techniques unambiguously confirms the formation in solution of a 2:1 binary lattice of tetrahedra and octahedra with $Fm\bar{3}m$ symmetry.

From the unit cell parameter $a_{FCC,}$ we can determine the distance between the nanoparticles. In this lattice, the quantity $a_{FCC}/\sqrt{2}$ corresponds to the edge length of the tetrahedral and octahedral volumes where both NPs fit. This edge length is larger than the edge lengths themselves, indicating that the packing in solution is not fully dense, leaving some room for solvent between the gold nanocrystals. Based on the known dimensions of the NPs (**Table S1**), we can evaluate the amount of solvent in-between the nanoparticles, taking into account as well the CTAC bilayer which is coating the gold surface. The packing fraction $\varphi = 0.63$ is obtained by dividing the volume occupied by the NPs (eight tetrahedra and four octahedra) divided by the volume of the FCC unit cell. This packing fraction does not take into account the minor truncation (**Figure S14**) in the volume estimations of the nanoparticles. In the binary assembly, all triangular facets of tetrahedra and octahedra are facing each other. From the value of the lattice parameter a_{FCC} and the known dimensions of the nanoparticles (**Table S1**), we can derive the inter-NPs distance d, which is the gap between the parallel facets of a tetrahedron facing an octahedron, including the CTAC bilayer coating ($d_B \approx 3.2$ nm) on each nanoparticle. We analyzed the distance between NPs (d) by SAXS (for wide range of concentrations) and LCTEM (50 and 150 mM) (**Figure 3B-C, S15-S16**) which are all in close agreement. This relatively large inter-particle spacing, more than two surfactants' bilayers ($2d_B \approx 6.4$ nm) (**Figure 3A**), results from the balance between attractive forces, depletion and Van der Waals interactions on one hand, and repulsive electrostatic interactions on the other hand. The resulting equilibrium distance, d^*, can be modelled analytically[31, 38] and is found to decrease as

the surfactant concentration increases, due to the major contribution of depletion forces (**Figure 3D-E, S17**). In line with the model, the inter-NP distance can be controlled by adjusting the concentration of surfactant (**Figure 3**).

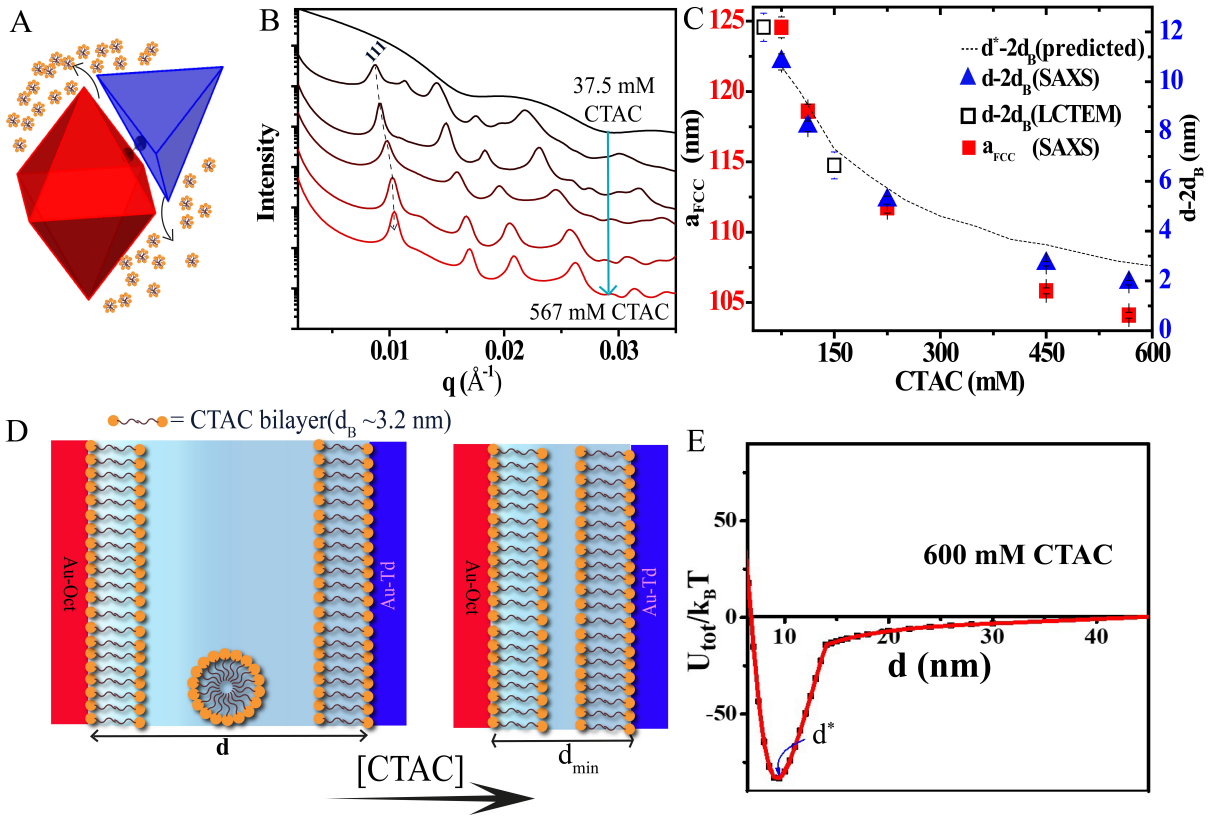

Figure 3: **Tunability of the supercrystal packing**: (A) Schematic diagram showing Au-Oct & Au-Td assembled by DISA. (B) 1D-SAXS pattern of the binary superlattices at different [CTAC] (75 mM to 567 mM). At 37.5 mM CTAC concentration, only the form factors of the dispersed NPs contributed to the signal, as no binary superlattice forms. Dashed line shows shift of <111> peak with [CTAC]. (C) Plot of the FCC unit cell parameter (a_{FCC}) and the inter-NP gap ((d-2d_B) (determined by SAXS, LCTEM) against CTAC concentration. Dashed line is the predicted value of (d^*-2d_B) from interaction potential. (D) Schematic diagram showing the change of the inter-NPs distance as a function of [CTAC]. The inter-NP distance *d* is the gap between the parallel facets of the Au-Td and Au-Oct, including the CTAC bilayers on each particle. d_{min} is the minimum inter-particle gap. (E) Plot of the theoretical interaction potential *vs.* inter-particle gap at 600 mM CTAC. d^* is the predicted inter-particle gap.

From 75 mM to 567 mM CTAC Bragg peaks corresponding to the $Fm\bar{3}m$ binary lattice were observed (**Figure 3B**) and *d* decreased from 17.2 nm to 8.3 nm (**Figure 3C**), which agrees well with calculated *d* spacing of 17.01 nm to 9.0 nm (**Figure S17**). Note that *d* tends toward the

minimum separation distance $2d_B$. This evolution is expected, since increasing surfactant concentration increases the osmotic pressure and weakens electrostatic repulsion by charge screening.[38] In this way, the packing fraction can be controlled in solution between φ=0.37 and φ=0.66 because of the relatively large inter-NP distances. In contrast, for the dry supercrystals imaged by SEM, packing fractions are essentially close to one.

So far, the size mismatch between the nanocrystal was about 4%, which is defined as $E.L._{Td}$-$E.L._{Oct}/E.L._{Oct}$. We then explored the possibility of forming the binary lattice with higher size mismatch (S.M.). To this end, Au-Oct with E.L = 47 nm were assembled with Au-Td of 48 nm (S.M. =3%), 52 nm (S.M. =10 %), 62 nm (S.M.= 31%) in separate experiments (**Figure 4, S18-19, Table S1**). While the mixtures with a S.M. up to 10 % formed a binary assembly, the one at S.M.=31% phase separated. This tolerance to size mismatch is interesting, meaning that the binary assembly is robust even when the triangular facets of the tetrahedra are larger than those of octahedra. We anticipate an upper limit for size mismatch of about 16.4% that correspond to the size difference between the actual nanoparticle and the one defined by the unit cell. Interestingly, in DISA, the nanoparticles are separated by solvent molecules, which contrasts with more conventional self-assembly methods where ligand flexibility, such as with DNA or alkanethiols, can accommodate size mismatches of similar amplitude.[14, 39]

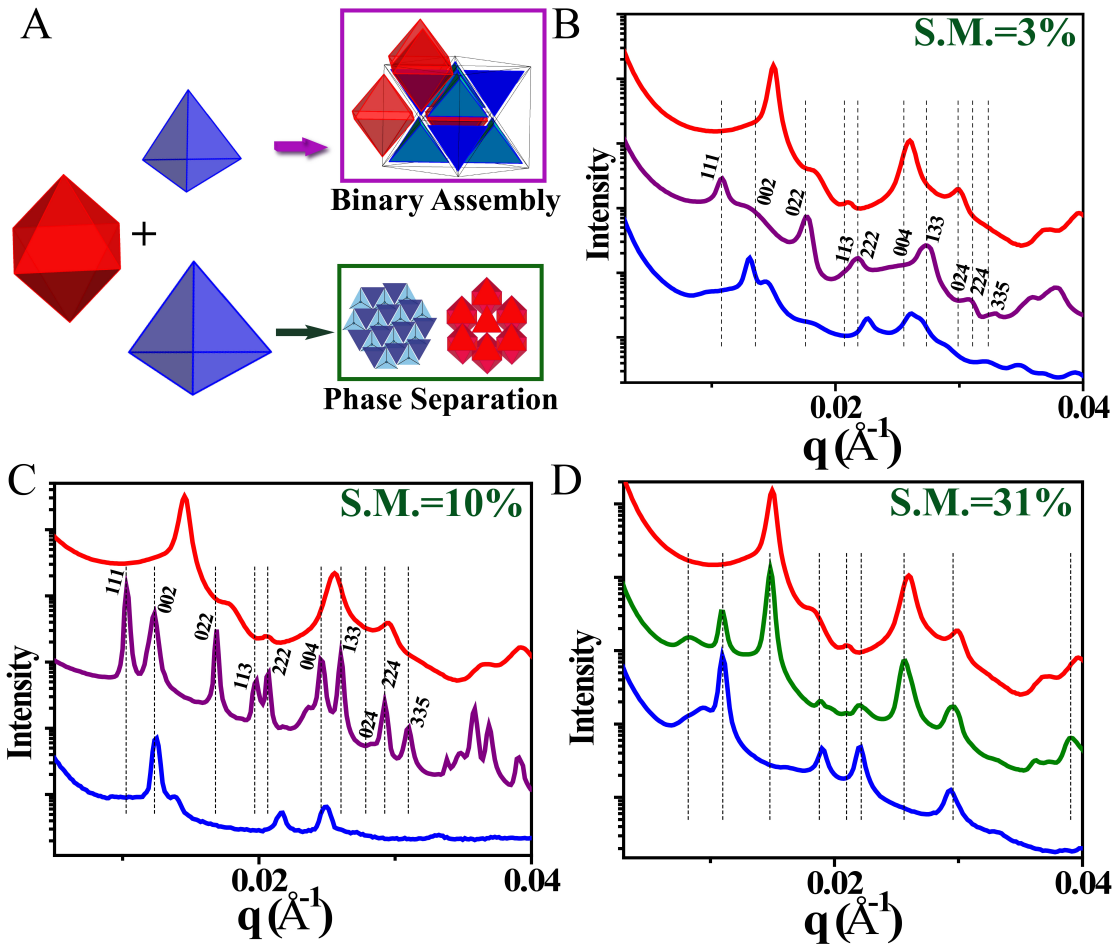

Figure 4: Effect of size mismatching on the binary lattice formation. A) Scheme showing either the formation of binary superlattice in case the edge length of the two shapes (Td-Oct) matches or phase separation in case the edge length of the two shapes mismatch. The 1D-SAXS patterns corresponding to tetrahedra and octahedra supercrystals are shown in red and blue respectively, and the curve in between them corresponds to the mixture supercrystals, which either form a binary lattice or phase separate. B) $E.L_{Oct}$ = 47 nm, $E.L_{Td}$ = 48 nm (S.M = 3 %): binary, C) $E.L_{Oct}$ =47 nm, $E.L_{Td}$ = 52 nm (S.M = 10 %): binary, D) $E.L_{Oct}$ = 47 nm, $E.L_{Td}$ = 62 nm (S.M = 31 %): phase separation.

So far, only a few examples have reported binary self-assembly with complementary shape nanoparticles using either slow evaporation-induced self-assembly or DNA base pairing. Here, we demonstrate the formation of a binary assembly of octahedra and tetrahedra with DISA into extended supercrystals with $Fm\bar{3}m$ symmetry. The binary assembly can be obtained in the dried state, forming large supercrystals with surfaces displaying triangular patterns and a packing fraction close to one (**Figure 1**). It can also be obtained in colloidal suspensions, as shown by SAXS and LCTEM analysis (**Figure 2**). We show that DISA can control the packing fraction

of such colloidal supercrystals between φ=0.37 and φ=0.66 (**Figure 3**), which is much lower than the dense space filling packing in the dry state. In principle, even lower packing fractions could be reached by extending the range of the depletion interaction using larger depletants. Conversely, coating the NPs with smaller ligands could yield higher packing fractions. Although the NPs have complementary shapes, DISA can achieve relatively low packing fractions, due to the presence of repulsive electrostatic interactions. In suspension, the binary assembly can be described as nanoparticles sitting in the middle of larger regions of the same shape (tetrahedra or octahedra) filled by the surfactant bilayer coating, solvent molecules and ions. Interestingly, this "empty" space can be controlled by the balance between the osmotic pressure and the repulsive electrostatic interactions. The FCC binary lattice formed by DISA is stabilized by two major effects: (a) without repulsive interactions, it maximizes the packing fraction (φ=1) compared to the case of unary supercrystals (φ=0.61 for tetrahedra and φ=0.89 for octahedra) that contain intrinsic geometrical voids. (b) the face-to-face interaction of all the triangular facets is maximized. Beyond the fundamental aspects, tuning the packing fraction in plasmonic supercrystals is relevant for controlling the accumulation of molecules in regions displaying intense optical activity. Our results show that DISA is efficient to co-assemble NPs with complementary shapes. These findings provide a deeper understanding of the self-assembly mechanisms in multicomponent systems and highlight the potential of DISA for creating complex and highly ordered nanomaterials with tailored properties.

Acknowledgement

The CNRS is acknowledged for funding and support. J. M. acknowledges financial support by the ANR NIMROD project (ANR-21-CE09-0019) for his PhD. R.N. and N.R. acknowledge financial support from the ANR METATRAP project (ANR-22-CE09-0011) for their post-doctoral positions. C.H. acknowledges financial support from the ANR CODENAME project (ANR-23-CE09-0032). The authors acknowledge SOLEIL for the provision of synchrotron radiation facilities (experiments 20231786 and 20221057) and we would like to thank Thomas Bizien for assistance in using beamline SWING. The present work had benefited from the electronic microscopy facility of Imagerie-Gif, (http://www.i2bc.parissaclay.fr), member of IBiSA (http://www.ibisa.net), supported by "France-BioImaging" (ANR10-INBS-04-01), and the Labex "Saclay Plant Science" (ANR-11-IDEX-0003-02). HRSEM was performed at the PLAMICS platform of the Institut Charles Sadron (ICS, Strasbourg, France). We are grateful to Region Ile-de-France for convention SESAME E1845, for the support of the JEOL ARM

200F electron microscope recently installed at the University Paris Cité where the liquid phase TEM experiments were conducted.

Supporting Information Available

The supporting information contains: the synthesis protocols of the gold nanoparticles, size analysis of the nanoparticles, calculation of the volume and ratio of Au-Td and Au-Oct, SAXS 2D pattern, SEM images of the self-assembled systems, LCTEM micrographs of the unary and binary assemblies, theoretical plot of interaction potential *vs.* inter-particle gap.

References

1. Cadotte, A. T.; Dshemuchadse, J.; Damasceno, P. F.; Newman, R. S.; Glotzer, S. C., Self-assembly of a space-tessellating structure in the binary system of hard tetrahedra and octahedra. *Soft Matter* **2016**, *12* (34), 7073-7078.
2. Conway, J. H.; Jiao, Y.; Torquato, S., New family of tilings of three-dimensional Euclidean space by tetrahedra and octahedra. *Proc. Nat. Acad. Sci. U.S.A.* **2011**, *108* (27), 11009-11012.
3. Deshpande, V. S.; Fleck, N. A.; Ashby, M. F., Effective properties of the octet-truss lattice material. *J. Mech. Phys. Solids* **2001**, *49* (8), 1747-1769.
4. Kovalenko, M. V.; Manna, L.; Cabot, A.; Hens, Z.; Talapin, D. V.; Kagan, C. R.; Klimov, V. I.; Rogach, A. L.; Reiss, P.; Milliron, D. J.; Guyot-Sionnnest, P.; Konstantatos, G.; Parak, W. J.; Hyeon, T.; Korgel, B. A.; Murray, C. B.; Heiss, W., Prospects of nanoscience with nanocrystals. *ACS Nano* **2015**, *9* (2), 1012-57.
5. Boles, M. A.; Engel, M.; Talapin, D. V., Self-Assembly of Colloidal Nanocrystals: From Intricate Structures to Functional Materials. *Chem. Rev.* **2016**, *116* (18), 11220-11289.
6. Talapin, D. V.; Lee, J.-S.; Kovalenko, M. V.; Shevchenko, E. V., Prospects of Colloidal Nanocrystals for Electronic and Optoelectronic Applications. *Chem. Rev.* **2009**, *110* (1), 389-458.
7. Herran, M.; Juergensen, S.; Kessens, M.; Hoeing, D.; Köppen, A.; Sousa-Castillo, A.; Parak, W. J.; Lange, H.; Reich, S.; Schulz, F.; Cortés , E., Plasmonic bimetallic two-dimensional supercrystals for H_2 generation. *Nat. Catal.* **2023**, *6* (12), 1205-1214.
8. Bodnarchuk, M. I.; Kovalenko, M. V.; Heiss, W.; Talapin, D. V., Energetic and Entropic Contributions to Self-Assembly of Binary Nanocrystal Superlattices: Temperature as the Structure-Directing Factor. *J. Am. Chem. Soc.* **2010**, *132* (34), 11967-11977.
9. Shevchenko, E. V.; Talapin, D. V.; Kotov, N. A.; O'Brien, S.; Murray, C. B., Structural diversity in binary nanoparticle superlattices. *Nature* **2006**, *439* (7072), 55-59.

10. Talapin, D. V.; Shevchenko, E. V.; Bodnarchuk, M. I.; Ye, X.; Chen, J.; Murray, C. B., Quasicrystalline order in self-assembled binary nanoparticle superlattices. *Nature* **2009**, *461* (7266), 964-967.

11. Dong, A.; Chen, J.; Vora, P. M.; Kikkawa, J. M.; Murray, C. B., Binary nanocrystal superlattice membranes self-assembled at the liquid-air interface. *Nature* **2010**, *466* (7305), 474-477.

12. Nagaoka, Y.; Wang, T.; Lynch, J.; LaMontagne, D.; Cao, Y. C., Binary Assembly of Colloidal Semiconductor Nanorods with Spherical Metal Nanoparticles. *Small* **2012**, *8* (6), 843-846.

13. Sánchez-Iglesias, A.; Grzelczak, M.; Pérez-Juste, J.; Liz-Marzán, L. M., Binary Self-Assembly of Gold Nanowires with Nanospheres and Nanorods. *Angew. Chem. Int. Ed.* **2010**, *49* (51), 9985-9989.

14. Lu, F.; Yager, K. G.; Zhang, Y.; Xin, H.; Gang, O., Superlattices assembled through shape-induced directional binding. *Nat. Commun.* **2015**, *6*.

15. Ye, X.; Millan, J. A.; Engel, M.; Chen, J.; Diroll, B. T.; Glotzer, S. C.; Murray, C. B., Shape Alloys of Nanorods and Nanospheres from Self-Assembly. *Nano Lett.* **2013**, *13* (10), 4980-8

16. Szustakiewicz, P.; Kowalska, N.; Bagiński, M.; Lewandowski, W., Active Plasmonics with Responsive, Binary Assemblies of Gold Nanorods and Nanospheres. *Nanomaterials* **2021**, *11* (9), 2296.

17. Paik, T.; Murray, C. B., Shape-Directed Binary Assembly of Anisotropic Nanoplates: A Nanocrystal Puzzle with Shape-Complementary Building Blocks. *Nano Lett.* **2013**, *13* (6), 2952-2956.

18. Sekh, T. V.; Cherniukh, I.; Kobiyama, E.; Sheehan, T. J.; Manoli, A.; Zhu, C.; Athanasiou, M.; Sergides, M.; Ortikova, O.; Rossell, M. D.; Bertolotti, F.; Guagliardi, A.; Masciocchi, N.; Erni, R.; Othonos, A.; Itskos, G.; Tisdale, W. A.; Stoferle, T.; Raino, G.; Bodnarchuk, M. I.; Kovalenko, M. V., All-Perovskite Multicomponent Nanocrystal Superlattices. *ACS Nano* **2024**, *18* (11), 8423-8436.

19. Cherniukh, I.; Rainò, G.; Stöferle, T.; Burian, M.; Travesset, A.; Naumenko, D.; Amenitsch, H.; Erni, R.; Mahrt, R. F.; Bodnarchuk, M. I.; Kovalenko, M. V., Perovskite-type superlattices from lead halide perovskite nanocubes. *Nature* **2021**, *593* (7860), 535-542.

20. Cherniukh, I.; Raino, G.; Sekh, T. V.; Zhu, C.; Shynkarenko, Y.; John, R. A.; Kobiyama, E.; Mahrt, R. F.; Stoferle, T.; Erni, R.; Kovalenko, M. V.; Bodnarchuk, M. I., Shape-Directed Co-Assembly of Lead Halide Perovskite Nanocubes with Dielectric Nanodisks into Binary Nanocrystal Superlattices. *ACS Nano* **2021**, *15* (10), 16488-16500.

21. Zhou, W.; Li, Y.; Je, K.; Vo, T.; Lin, H.; Partridge, B. E.; Huang, Z.; Glotzer, S. C.; Mirkin, C. A., Space-tiled colloidal crystals from DNA-forced shape-complementary polyhedra pairing. *Science* **2024**, *383* (6680), 312-319.
22. van Anders, G.; Klotsa, D.; Ahmed, N. K.; Engel, M.; Glotzer, S. C., Understanding shape entropy through local dense packing. *Proc. Nat. Acad. Sci. U.S.A.* **2014**, *111* (45), E4812-E4821.
23. Young, K. L.; Personick, M. L.; Engel, M.; Damasceno, P. F.; Barnaby, S. N.; Bleher, R.; Li, T.; Glotzer, S. C.; Lee, B.; Mirkin, C. A., A Directional Entropic Force Approach to Assemble Anisotropic Nanoparticles into Superlattices. *Angew. Chem. Int. Ed.* **2013**, *52* (52), 13980-13984.
24. Vo, T.; Glotzer, S. C., A theory of entropic bonding. *Proc. Nat. Acad. Sci. U.S.A.* **2022**, *119* (4), e2116414119.
25. Lekkerkerker, H. N. W.; Tuinier, R., Depletion Interaction. In *Colloids and the Depletion Interaction*, Springer Netherlands: Dordrecht, 2011; pp 57-108.
26. Jana, N. R., Nanorod shape separation using surfactant assisted self-assembly. *Chem. Commun.* **2003**, (15), 1950-1951.
27. Park, K.; Koerner, H.; Vaia, R. A., Depletion-Induced Shape and Size Selection of Gold Nanoparticles. *Nano Lett.* **2010**, *10* (4), 1433-1439.
28. Baranov, D.; Fiore, A.; van Huis, M.; Giannini, C.; Falqui, A.; Lafont, U.; Zandbergen, H.; Zanella, M.; Cingolani, R.; Manna, L., Assembly of Colloidal Semiconductor Nanorods in Solution by Depletion Attraction. *Nano Lett.* **2010**, *10* (2), 743-749.
29. Yang, P. W.; Thoka, S.; Lin, P. C.; Su, C. J.; Sheu, H. S.; Huang, M. H.; Jeng, U. S., Tracing the Surfactant-Mediated Nucleation, Growth, and Superpacking of Gold Supercrystals Using Time and Spatially Resolved X-ray Scattering. *Langmuir* **2017**, *33* (13), 3253-3261.
30. Yang,C.-W.; Chiu,C.-Y., Huang, M. H., Formation of Free-Standing Supercrystals from the Assembly of Polyhedral Gold Nanocrystals by Surfactant Diffusion in the Solution. *Chem. Mat.* **2014**, *26* (16), 4882-4888.
31. Young, K. L.; Jones, M. R.; Zhang, J.; Macfarlane, R. J.; Esquivel-Sirvent, R.; Nap, R. J.; Wu, J.; Schatz, G. C.; Lee, B.; Mirkin, C. A., Assembly of reconfigurable one-dimensional colloidal superlattices due to a synergy of fundamental nanoscale forces. *Proc. Nat. Acad. Sci. U.S.A.* **2012**, *109* (7), 2240-5.
32. Sacanna, S.; Pine, D. J.; Yi, G.-R., Engineering shape: the novel geometries of colloidal self-assembly. *Soft Matter* **2013**, *9* (34), 8096-8106.

33. Sacanna, S.; Irvine, W. T. M.; Chaikin, P. M.; Pine, D. J., Lock and key colloids. *Nature* **2010**, *464* (7288), 575-578.

34. Scarabelli, L.; Sánchez-Iglesias, A.; Pérez-Juste, J.; Liz-Marzán, L. M., A "Tips and Tricks" Practical Guide to the Synthesis of Gold Nanorods. *J. Phys. Chem. Lett.* **2015**, *6* (21), 4270-4279.

35. Wang, Y.; Chen, J.; Zhong, Y.; Jeong, S.; Li, R.; Ye, X., Structural Diversity in Dimension-Controlled Assemblies of Tetrahedral Gold Nanocrystals. *J. Am. Chem. Soc.* **2022**, *144* (30), 13538-13546.

36. García-Lojo, D.; Modin, E.; Gómez-Graña, S.; Impéror-Clerc, M.; Chuvilin, A.; Pastoriza-Santos, I.; Pérez-Juste, J.; Constantin, D.; Hamon, C., Structure and Formation Kinetics of Millimeter-Size Single Domain Supercrystals. *Adv. Funct. Mater.* **2021**, *31* (27), 2101869.

37. Goldmann, C.; Chaabani, W.; Hotton, C.; Imperor-Clerc, M.; Moncomble, A.; Constantin, D.; Alloyeau, D.; Hamon, C., Confinement Effects on the Structure of Entropy-Induced Supercrystals. *Small* **2023**, *19* (44), e2303380.

38. Cheng, Z.; Jones, M. R., Assembly of planar chiral superlattices from achiral building blocks. *Nat. Commun.* **2022**, *13* (1), 4207.

39. Shevchenko, E. V.; Talapin, D. V.; Murray, C. B.; O'Brien, S., Structural Characterization of Self-Assembled Multifunctional Binary Nanoparticle Superlattices. *J. Am. Chem. Soc.* **2006**, *128* (11), 3620-3637.

TOC